

# A Wireless Geophone Network Architecture using IEEE 802.11af with Power Saving Schemes

Varun Amar Reddy, *Student Member, IEEE*, Gordon L. Stuber, *Fellow, IEEE*,  
Suhail Al-Dharrab, *Member, IEEE*, Wessam Mesbah, Ali Hussein Muqaibel

**Abstract**—Seismic surveys are conducted by oil exploration companies to keep up with the global demand for oil and gas. Although seismic cables offer fast and reliable data transfer, they account for a majority of the equipment weight, logistics, and labor costs. A novel wireless geophone network architecture, compliant with the IEEE 802.11af standard, is described. Operation in television white spaces can achieve long transmission ranges, allowing for scalable coverage of large seismic survey areas. Two methods for data collection are proposed: a Geophone-Polling (GP) scheme and an Adaptive Geophone Time Division Multiple Access Scheduling (AGTS) scheme. The two schemes are analyzed and evaluated in terms of the total time taken for data acquisition and the average power consumption, in comparison to the default IEEE 802.11 channel access schemes. The problem of hexagonal clustering for orthogonal deployment of geophones is also tackled, and the impact of co-channel interference is considered. The proposed schemes not only reduce data acquisition time, but also the average power consumption of the geophones, thereby improving the lifetime of wireless seismic surveys.

**Index Terms**—seismic measurements, wireless geophone networks, wireless LAN, access protocols, power saving.

## I. INTRODUCTION

Seismic surveys help acquire detailed images of the various layers of the Earth's subsurface in order to determine the location and size of oil and gas reservoirs. A seismic source is used to generate variable-frequency waves that are reflected by subsurface layers. The reflected waves are detected by devices called *geophones*, that are deployed across the survey area. The data recorded by the geophones is processed to generate a visual image of the Earth's subsurface.

The subject of 2-D and 3-D seismic survey design has been well studied in [1], [2]. A typical survey can deploy 10,000–30,000 geophones, covering an area of up to 100 km<sup>2</sup>. Given the sheer size of a seismic survey, the use of cable to connect all geophones accounts for a majority of the equipment weight and cost. Although cable can offer high data rates in a reliable manner, a significant amount of time is spent in troubleshooting problems pertaining to the cables and connectors. The use of a wireless geophone network would eliminate the problems associated with laying of cables in

This work is supported by the Center for Energy and Geo Processing at Georgia Institute of Technology and King Fahd University of Petroleum and Minerals, under grant number GTEC1601.

V. A. Reddy and G. L. Stuber are with the School of Electrical and Computer Engineering, Georgia Institute of Technology, Atlanta, GA 30332, USA (e-mail: varun.reddy@gatech.edu; stuber@ece.gatech.edu).

S. Al-Dharrab, W. Mesbah, and A. H. Muqaibel are with the Electrical Engineering Department, King Fahd University of Petroleum and Minerals, Dhahran 31261, Saudi Arabia (e-mail: suhaild@kfupm.edu.sa; mesbahw@gmail.com; muqaibel@kfupm.edu.sa).

undulated terrain. More importantly, there is a far less impact on the environment, as cables can directly affect the flora and fauna of the region.

While wireless systems offer an excellent alternative to cable, they come with the challenging task of achieving high data rates over a widespread area in an energy-efficient manner. Given a seismic wavefield sampling time of 0.5 ms, a geophone with a 24-bit Analog-to-Digital Converter (ADC) would generate data at a rate of 48 kbps. Three-component (3-C) geophones would generate thrice the amount of data, at a rate of 144 kbps. Although the data rate per seismic channel may not be significantly large, the aggregate rate for say 30,000 geophones, can be several Gigabits per second. Additionally, power saving schemes must be incorporated into the wireless systems since seismic acquisition can be conducted for durations lasting up to 30 days.

Several works have proposed techniques for power saving in wireless seismic data acquisition. Savazzi et al. proposed a hierarchical architecture in [3] and discussed the viability of using ZigBee, Bluetooth, Ultra-Wideband (UWB), WiFi, and WiMAX. A more thorough description of the UWB-based architecture is provided in [4], wherein geophones transfer data to nearby cluster heads, which in turn relay the data to a gateway node and subsequently to a central recording unit. Power saving is achieved through the use of low-power UWB radios and distributed beaconing derived from the ECMA-368 standard, albeit with significant modifications to the ECMA framing structure. Additionally, non-uniform power consumption is introduced wherein the cluster heads that are closest to the gateways are required to relay the most amount of traffic. In [5], a cross-layer design involving the routing policy, resource allocation via time division multiple access (TDMA), and data compression is investigated for a multi-hop network. A convex optimization problem is set up with the objective of minimizing the energy consumption. Power saving techniques have also been considered in [6], in which a TDMA-based service period access scheme, derived from the IEEE 802.11ad standard, is used over 60 GHz channels for acquiring seismic data. The geophones are operated in sleep mode outside their designated time slots.

In addition to the aforementioned literature, several works have applied wireless sensor networks to perform seismic data acquisition. A wireless architecture is described in [7] wherein seismic data is relayed serially along a chain of geophones using multiplexing schemes such as frequency division multiplexing. However, acquisition time may be high and uniform power consumption among the geophones is a

cause for concern. The authors in [8] proposed an architecture for relaying data through a chain-type sensor network for long-range monitoring and analyzed its performance. To facilitate the relaying process, a number of redundant cluster heads in the same region would be required, which can disrupt the standard topology in which the geophones are required to be deployed. Moreover, the above ‘chain-type’ approaches would neither scale with the number of geophones nor the data generation rates. In [9], data is acquired from a cluster of geophones by relay nodes using TDMA, and is subsequently transferred to a central recording unit using directional antennas. The use of full-duplex radios and antenna arrays has also been suggested for the relay nodes. However, a large number of relay nodes may be required to cover the survey area and a high power consumption may arise from the beamforming process. A more recent experimental study based on an Internet-of-Things network was carried out by Jamali-Rad et al. [10]. An economical low-power wireless architecture based on Long Range (LoRa) technology is proposed for seismic quality control, but is not directed towards data-intensive seismic acquisition. Consequently, low data generation rates and a sparse deployment of geophones are assumed. Overall, the above methods suffer from the problems of scalability in addition to effective and uniform power conservation across the geophone network. Some of the schemes may also be proprietary, as they combine the use of elements taken from multiple standards, rendering them more expensive and inaccessible.

This paper introduces a novel geophone network architecture, compliant with the relatively new IEEE 802.11af standard, that provides the requisite data rates over large areas and efficient power saving with a minimal number of gateway devices. Our previous work presented in [11] is extended in this paper to include an analysis of the GP scheme and simulation results with an improved interference model. Additional simulation results are provided after considering the impact of co-channel interference, an aspect that has not been taken into account in prior work. Furthermore, the power saving strategy in the GP scheme relies on the current status of the Network Allocation Vector (NAV) timer. The NAV metric is not exposed by most 802.11 Network Interface Cards (NICs) to the higher layers. Although this can be achieved by sufficient modification of the device drivers, an Adaptive Geophone Time Division Multiple Access Scheduling (AGTS) scheme is proposed, that not only requires minimal changes to the drivers but also offers improved power saving. This is motivated by the simple notion that power saving efficiency is improved when the transmission schedule is known to all geophones. However, this comes at the cost of a larger amount of time required for data collection.

The remainder of this paper is organized as follows. The proposed network architecture and topology are described in Section II. The GP and AGTS schemes are described and analyzed in Sections III and IV respectively. In Section V, an additional data collection scheme is discussed that can be applied concurrently with the seismic recording process. Simulation results are provided in Section VI wherein the trade-off between the GP and AGTS schemes is seen and

suitable operating parameters for the proposed architecture are obtained. The findings are then summarized and evaluated in the conclusion in Section VII.

## II. PROPOSED NETWORK ARCHITECTURE

Following a brief discussion of the IEEE 802.11af standard, a description of the architecture is offered in Section II.A, along with the seismic surveying methodology and its impact on the overall network topology in Section II.B.

The IEEE 802.11af standard [12], [13] is an attractive option for establishing wireless coverage across seismic survey areas. The standard operates in the TVWS (television white space) bands, which are unallocated frequencies that are otherwise used for digital television broadcast transmissions. The TVWS bands range between 50 MHz and 700 MHz in North America, and between 54 MHz and 698 MHz in Europe [12]. Owing to lower frequencies, non-line-of-sight coverage is enhanced and the transmission range is significantly increased, as compared to the 2.4 GHz and 5 GHz ISM bands. This increase in transmission range can be exploited to provide coverage over large areas with minimal number of access points or gateway devices. Seismic surveys for oil exploration are typically carried out in remote locations, away from urban areas. Consequently, white space spectrum would be plentiful, as compared to higher frequency bands such as 2.4 GHz, 5 GHz, and mm-wave, hence allowing operation with a large amount of bandwidth. Other standardization efforts have been made for operation in TVWS bands, such as the IEEE 802.15.4m, IEEE 802.22, and ECMA-392 standards. Comparatively, the IEEE 802.11af standard offers better performance in terms of throughput [14]–[16], and is easier to set up.

### A. A Hierarchical Architecture

Fig. 1 provides an illustration of the proposed architecture based on the IEEE 802.11af standard. Wireless coverage is provided by *Wireless Gateway Nodes (WGNs)* that collect data from all the geophones within transmission range. The information collected by the WGNs is then relayed to the *Data Collection Center (DCC)*, which is supported by a taller antenna.

A star topology is preferable, as the geophones would not have to spend additional energy on relaying information through a multi-hop network. The WGNs can instead be provided with larger storage and energy capabilities in order to improve the lifetime of the geophones. A star topology is more robust to geophone failures which would otherwise hinder data transfer in a relay-based ad hoc architecture. Additionally, a star topology can achieve a synchronization accuracy well below 10  $\mu$ s, which is a desirable value for the maximum timing skew in geophone networks [4], as compared to ad hoc mode of operation wherein synchronization messages are exchanged in a peer-to-peer manner.

Abiding by the conventions laid out by the IEEE 802.11af standard [12], [13], the DCC would act as the *Registered Location Secure Server (RLSS)*, which is a local database that stores the operating parameters and the geographic location for a small number of Basic Service Sets (BSSs). The WGNs

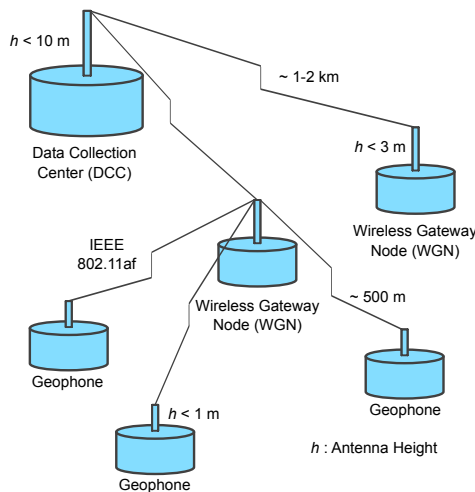


Fig. 1: Proposed Network Architecture

would serve as *geolocation database dependent enabling stations*, that supervise the working of the geophones in their respective BSSs, as per the operating parameters obtained from the RLSS. The IEEE 802.11af standard operates through the Television Very High Throughput (TVHT) PHY [12]. This mandates the use of channel bandwidths of 6, 7, or 8 MHz. Channel bonding can also be employed, between contiguous or non-contiguous channels, each of width  $W$ , to yield total channel bandwidths of  $2W$  or  $4W$ .

### B. Seismic Survey Process and Network Topology

Following a description of the proposed network architecture, the subject of the geophone network topology is considered here. An understanding of the seismic survey process is essential to determining the geophone network topology, with denser topologies resulting in superior image quality. Geophones are typically positioned 5-30 meters apart along a straight line, to form a *Receiver Line (RL)*. Vibroseis trucks move along the *Source Line (SL)* and generate seismic waves, or a *sweep*, for a duration of 4-12 s, known as the *sweep length*. Data is recorded by the geophones for a duration known as the *listen interval*. During a *move-up interval* of 8-10 s, the vibroseis trucks move to the next point where a sweep will be conducted. The sweep, listen, and move-up operations are repeated periodically across the survey area [17].

Two types of seismic surveying methods are considered in this analysis. A *single-fleet* operation involves a single vibroseis truck that conducts sweeps across the area. To improve productivity, multiple vibroseis trucks may be deployed to conduct overlapping sweeps, so long as they are separated sufficiently in distance. *Flip-flop* operations involve a pair of trucks, wherein the second truck begins a sweep immediately after the listen interval of the first truck's sweep. Hence, flip-flop operations are able to sweep the survey area more quickly, at a rate of 145 sweeps/hour as compared to 95 sweeps/hour in single-fleet operations [18]. However, by reducing the time period available for data acquisition between consecutive sweeps, real-time acquisition is more challenging to achieve in flip-flop operations.

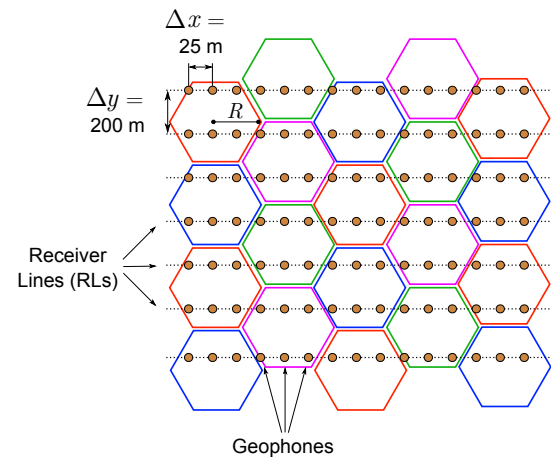


Fig. 2: Orthogonal Deployment of Geophones with a 4-cell Frequency Reuse Pattern

An orthogonal geometry is considered [1] in this analysis, wherein the RLs and SLs are perpendicular to one another. Fig. 2 depicts a topology that specifies an inter-geophone distance of 25 m along the RL, and an inter-RL distance of 200 m. A total of 30 RLs, each comprising 480 geophones, yields a total of 14,400 geophones that span an area of approximately 72 km<sup>2</sup>.

Wireless coverage can be provided through frequency reuse by dividing the seismic survey area into tessellating hexagonal cells [19], with each cell containing a single WGN. Let  $R$  be the radius of the hexagonal cells,  $X$  be the number of geophones in a single RL,  $Y$  be the total number of RLs,  $\Delta x$  be the spacing between geophones, and  $\Delta y$  be the spacing between the RLs. A correction to the counting formula in [11] for the total number of required WGNs,  $N$ , yields the following expression.

$$N = \begin{cases} 2\lceil y_c \rceil \lfloor x_c \rfloor + \lceil y_c \rceil & \{y_c\} \leq 1/2, \{x_c\} \leq 1/3 \\ 2\lceil y_c \rceil \lceil x_c \rceil & \{y_c\} \leq 1/2, \{x_c\} > 1/3 \\ (2\lceil y_c \rceil + 1)\lfloor x_c \rfloor + \lceil y_c \rceil & \{y_c\} > 1/2, \{x_c\} \leq 1/3 \\ (2\lceil y_c \rceil + 1)\lceil x_c \rceil & \{y_c\} > 1/2, \{x_c\} > 1/3 \end{cases} \quad (1)$$

where  $y_c = \Delta y \cdot (Y - 1) / (\sqrt{3} \cdot R)$ ,  $x_c = \Delta x \cdot (X - 1) / (3 \cdot R)$ , and  $\lceil \alpha \rceil$ ,  $\lfloor \alpha \rceil$ ,  $\{\alpha\}$  denote the ceiling, floor, and fractional part of  $\alpha$  respectively.

### III. GP SCHEME

Given the acquisition time and power consumption constraints, there is a need for a specialized channel access scheme in wireless geophone networks. The default access scheme provided by the 802.11af Medium Access Control (MAC) layer is the *Distributed Coordination Function (DCF)* [20], wherein the Carrier Sense Multiple Access with Collision Avoidance (CSMA/CA) scheme along with binary exponential backoff is employed. At each transmission attempt, the backoff time  $b$  depends on the contention window size ( $CW$ ) and the slot time ( $T_{slot}$ ).

$$b = Rand \times T_{slot} \quad (2)$$

where *Rand* denotes a random integer that is uniformly distributed in the interval  $[0, CW-1]$ . The value of  $CW$

ranges between  $CW_{\min}$  and  $CW_{\max}$ . Upon the occurrence of a failed transmission, the  $CW$  is doubled in value until the transmission finally succeeds, in which case  $CW$  is reset back to  $CW_{\min}$ . Consequently, in the presence of a large number of geophones in a single BSS, the  $CW$  can rapidly double in value, which in turn can lead to relatively long backoff times, as can be deduced from (2). The *Point Coordination Function* (PCF) [20] can help reduce the delay associated with large backoff times by providing contention-free access. As the *point coordinator*, the WGN can designate a Contention Period (CP) where the DCF is used, and a Contention-Free Period (CFP) where the PCF is used. During the CFP, each geophone is polled by the WGN with a *CF-POLL* frame and granted contention-free channel access. However, excessive control signalling is done in PCF, which in turn does not scale with the number of geophones in a single BSS. For instance, geophones that have already transmitted their data continue to be polled by the WGN, which simply respond with a *CF-ACK* frame. This creates a delay for subsequent geophones on the polling list. Let  $d$  be the delay associated with the  $i^{\text{th}}$  geophone on the polling list before it can send a data frame.

$$d \geq (i - 1) \times [T_{CF-POLL} + T_{CF-ACK}] \quad (3)$$

where  $T_{CF-POLL}$  and  $T_{CF-ACK}$  denote the time taken to transmit the *CF-POLL* and *CF-ACK* frames respectively. For a large number of geophones, the corresponding polling list is long and  $d$  can attain relatively large values. Note that complete data transfer would involve the transmission of several frames from each geophone;  $d$  characterizes the delay associated with just one frame. Overall, the default channel access schemes, DCF and PCF, are not feasible methods for data collection from geophone networks.

A *Geophone Polling (GP)* scheme is proposed for data collection from the geophones. This protocol would operate over the lower PHY/MAC layers of the architecture, with functionality being implemented at the higher transport and application layers. While the GP scheme has been discussed previously in [11], the average power consumption shows an increasing trend with the WGN cell radius. This arises from the fact that only *Request-to-Send (RTS)* frames were used for updating the duration of sleep, while this work also takes into account the *Clear-to-Send (CTS)* frames. Furthermore, a time and power consumption analysis is conducted, after a brief summary of the key features and operation of the GP scheme.

#### A. Key Features

1) *Providing Contention-Free Access*: The proposed GP scheme aims to offer each geophone the requisite amount of contention-free time resources to complete data transfer with minimal overhead, thereby countering the problems associated with large values of  $b$  and  $d$ .

2) *Transmission Control Protocol (TCP) Fairness*: TCP fairness is of significant concern in 802.11 networks when several TCP connections are operated through a single access point [21], [22]. To counter this effect, the GP scheme allows only a single TCP flow to operate at any point of time.

3) *Power Saving*: Power is conserved through the GP scheme by letting the geophones operate in sleep mode (transceiver is switched off) in order to avoid idle listening (listening to the channel when there are no ongoing transmissions) and packet overhearing (listening to ongoing transmissions between other geophones). For instance, a geophone can enter sleep mode after its data has been successfully transmitted.

4) *Open Standard*: All functionality is implemented at the application and transport layers. Consequently, the proposed architecture is compliant with the IEEE 802.11af standard.

#### B. Operation

The proposed GP scheme operates through the services of the DCF. User Datagram Protocol (UDP) packets are utilized by the WGN for signalling the individual geophones. A single UDP packet from the WGN would mark the beginning of data transmission from a geophone, unlike the case in PCF, where every data frame is sent only after a *CF-POLL* frame is received. Subsequent UDP packets are used to instruct a geophone to enter sleep mode, after the completion of its data transfer. UDP packets are ideal for this application as they do not consume much bandwidth (by limiting the packet size to be on the order of a few bytes) and they do not require an acknowledgment from the recipient at the transport layer. In Fig. 3, an illustration of the GP scheme is provided, whose operation is described in the following steps.

- 1) A schedule is created by the WGN to determine the order in which geophones are signalled for data transmission.
- 2) Data transmission using TCP is triggered from the geophone  $G_a$  upon the reception of a UDP packet,  $U_s$ .
- 3) All geophones, apart from  $G_a$ , that can hear the exchange of frames between the WGN and  $G_a$  update their NAV counter accordingly. The duration values contained in the headers of the RTS (request to send) and CTS (clear to send) frames can be used to determine the duration of sleep, as seen in Fig. 3. The concept of power-saving using the NAV metric has been previously studied in [23]–[25]. A duration of 250  $\mu\text{s}$  is required to switch from sleep to idle mode of operation [25], [26]. A geophone can be timed to wake up before the expiration of the NAV counter.
- 4) The TCP connection with  $G_a$  is terminated by the WGN when data transfer is complete.  $G_b$  is now signalled with a  $U_s$  packet for data transmission. Thus, only a single TCP connection is open at any point of time.
- 5) A UDP packet,  $U_{sl}$ , is also sent by the WGN to  $G_a$  indicating it to enter sleep mode, for a duration until the start of the next sweep. This is acknowledged by  $G_a$  through the UDP packet  $U_{sla}$ .

Steps (2–5) are repeated in order of the schedule until data acquisition from all geophones is completed. A unique schedule is drawn from the uniform distribution for each sweep, to ensure uniform power consumption among all geophones over several sweeps, as shown in Appendix A.

#### C. Time Analysis

Prior to conducting an analysis of the total time required for data collection, a model for computing the amount of data

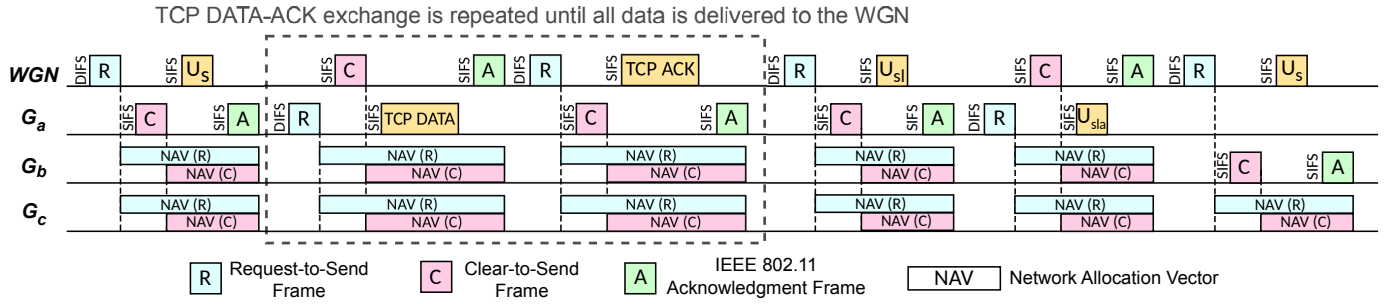


Fig. 3: A Timing Diagram for the Geophone-Polling Scheme.

received over a given duration of time is desired. This can be achieved through the use of a semi-Markov Process [27], wherein a certain amount of time is spent in a given state before transitioning to the next state of the Markov process.

Delayed TCP acknowledgments are considered in this analysis; a feature that is commonly employed in open source Linux kernel implementations of TCP. As stated in RFC 1122 [28], a single TCP acknowledgment is sufficient for at most two TCP payload segments, thereby reducing the total number of required acknowledgments and facilitating higher TCP throughput. Hence, two states,  $P_1$  and  $P_2$ , are used to represent the transmission of two consecutive TCP payload segments from a geophone, as shown in Fig. 4. The state  $A$  represents the transmission of a TCP acknowledgment by the WGN, and the state  $C$  represents a collision wherein a transmission of neither payload nor acknowledgment occurs. Thus, the model represents the cyclic transmission of two TCP payload segments followed by a TCP acknowledgment. Note that each state comprises the transmission of the requisite management frames at the MAC layer.

As seen in Fig. 4, the transition probabilities are a function of  $p$ , which represents the collision probability of frames at the MAC layer. When the exchange of RTS-CTS frames is employed, it is sufficient to consider the collision probability of RTS frames alone, since the channel is reserved through virtual carrier sensing for the remaining frames within a state [29]. Before delving into the finer details of the Markov process depicted in Fig. 4, a digression is made into the behavior of the collision probability  $p$ .

The GP scheme enforces its functionality at the higher layers, while continuing to employ the DCF at the MAC layer. Since channel access to each of the geophones is scheduled sequentially by the WGN, implying that only a single geophone

would be operational at any given point of time, any collisions would solely arise between the transmissions of the presently scheduled geophone and the WGN. Under the assumption of saturated traffic at the geophones, meaning that there are always data segments ready for transfer to the WGN, the traffic at the WGN can also be assumed to be saturated since the corresponding TCP acknowledgments need to be sent back to the geophones [30]. Consequently, for a single TCP link between a geophone and the WGN, contention between the transmission of TCP payload segments and the corresponding TCP acknowledgments would be observed. More precisely, the contention results in collisions that occur when the backoff counters of the geophone and the WGN reach zero in the same slot. A methodology for computing the collision probability  $p$  in such a scenario is provided via a fixed point analysis for saturated traffic over the DCF [31]. As derived in [31], the average contention window size  $CW_{avg}$  is expressed in (4) as a weighted sum of the average backoff window for each retransmission attempt at the MAC layer, up to a maximum of  $K$  retransmissions such that  $CW_{max} = 2^{K-1} \cdot CW_{min}$ . The value of  $CW_{avg}$  is then used to determine  $p$  in (5), by computing the probability of a transmission from any of the other  $n - 1$  stations during the transmission of a reference station. Hence, equations (4) and (5) are set up to yield solutions for  $p$  and  $CW_{avg}$ . In our scenario,  $n$  is simply equal to 2, since only a single geophone and the WGN are involved in the contention process at any given point of time.

$$CW_{avg} = \left( \frac{1-p}{1-p^K} \right) \sum_{m=0}^{K-1} p^m \cdot \left( \frac{2^m \cdot CW_{min} - 1}{2} \right) \quad (4)$$

$$p = 1 - (1 - 1/CW_{avg})^{n-1} \quad (5)$$

Returning to the model depicted in Fig. 4, each of the four states is associated with a certain average duration of time.

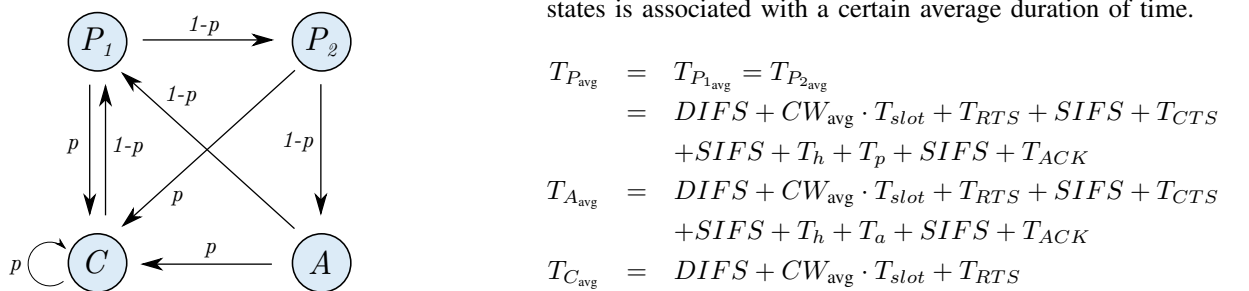


Fig. 4: Markov Model for TCP Data Transmission

The various notations are specified in Table I. Given the

TABLE I: Definition of Time-Specific Parameters

Notation	Description
SIFS	Short Interframe Space
PIFS	Point Coordination Function Interframe Space
DIFS	Distributed Coordination Function Interframe Space
$T_{slot}$	Slot Time
$T_{RTS}$	Transmission time of an RTS frame
$T_{CTS}$	Transmission time of an CTS frame
$T_{ACK}$	Transmission time of an IEEE 802.11 acknowledgment frame
$T_h$	Transmission time of header of a data frame
$T_p$	Transmission time of payload of a data frame (TCP data)
$T_a$	Transmission time of payload of a data frame (TCP acknowledgement)
$T_u$	Transmission time of payload of a data frame (UDP packet)

transition probabilities between the states in Fig. 4, the steady-state probability of state  $i$ , say  $\phi_i$ , can be found.

$$\begin{aligned}\phi_{P_1} &= \frac{p \cdot (1-p)}{1 - (1-p)^3} & \phi_{P_2} &= \frac{p \cdot (1-p)^2}{1 - (1-p)^3} \\ \phi_A &= \frac{p \cdot (1-p)^3}{1 - (1-p)^3} & \phi_C &= p\end{aligned}$$

Let  $\pi_i$  denote the proportion of time that the semi-Markov process spends in state  $i$ .  $\pi_i$  can be expressed as the weighted average of the steady-state probabilities, where the weights are given by the duration spent in each state [27].

$$\pi_i = \frac{\phi_i \cdot T_i}{\sum_j \phi_j \cdot T_j} \quad (6)$$

where  $j$  is summed over all the states of the process.

The amount of data transmitted in a given duration  $t$  can be computed by scaling the number of times that the states  $P_1$  and  $P_2$  is entered, with the mean value of the payload size,  $E(P)$ .

$$\text{Data transmitted} = \left\{ \frac{(\pi_{P_1} + \pi_{P_2}) \cdot t}{T_{P_{avg}}} \right\} \cdot E(P) \quad (7)$$

The GP scheme allows each geophone to transmit all of its data until completion. The maximum amount of time required by the  $g^{th}$  geophone for data transfer can be denoted by  $\tau_g$ , using which the total amount of time  $\tau$  can be computed.

$$\tau_g = 3 \cdot T_U + \left( \frac{D \cdot T_{P_{avg}}}{E(P) \cdot (\pi_{P_1} + \pi_{P_2})} \right) \quad (8)$$

$$\tau = \sum_{g=1}^G \tau_g \quad (9)$$

where  $T_U$  represents the time required for the transmission of a UDP packet,  $D$  denotes the total amount of data to be transmitted by each of the geophones, and  $G$  is the total number of geophones in the BSS. A factor of 3 is used in (8) to account for each of the three types of UDP packets that are used for signalling i.e.  $U_s$ ,  $U_{sl}$ , and  $U_{sla}$ , as seen in Fig. 3. Note that there is no contention for the transmission of a UDP packet, since an acknowledgment from the receiver is not required.

$$\begin{aligned}T_U &= DIFS + (CW_{min} - 1)/2 \cdot T_{slot} + T_{RTS} + SIFS \\ &\quad + T_{CTS} + SIFS + T_h + T_u + SIFS + T_{ACK}\end{aligned}$$

#### D. Power Consumption Analysis

The time analysis presented in the previous section can be extended to power consumption as well. During the inter frame spaces and backoff period, a geophone will operate in idle mode. When a packet is either being transmitted or received, a geophone will operate in the transmit or receive mode respectively. To conserve power when a geophone is not required to send or receive data, such as in the duration after data transfer, the transceiver can be powered off and the geophone operated in sleep mode.

Let  $V$  denote the supply voltage, and  $I_{tx}$ ,  $I_{rx}$ ,  $I_{idle}$ ,  $I_{sl}$  denote the current drawn while operating in transmit, receive, idle, and sleep modes respectively. Let the amount of energy consumed by the  $g^{th}$  geophone during its data transfer be denoted by  $E_{g,d}$ .

$$\begin{aligned}E_{g,d}^U &= (T_{RTS} + T_h + T_u + 2 \cdot (T_{CTS} + T_{ACK})) \cdot I_{tx} \cdot V \\ &\quad + (2 \cdot (T_{RTS} + T_h + T_u) + T_{CTS} + T_{ACK}) \cdot I_{rx} \cdot V \\ &\quad + 3 \cdot (DIFS + (CW_{min} - 1)/2 \cdot T_{slot} \\ &\quad + 3 \cdot SIFS) \cdot I_{idle} \cdot V \\ E_{g,d}^P &= \left( \frac{(\pi_{P_1} + \pi_{P_2}) \cdot (\tau_g - 3 \cdot T_U)}{T_{P_{avg}}} \right) \{(T_{RTS} + T_h + T_p) \cdot I_{tx} \cdot V + (T_{CTS} + T_{ACK}) \cdot I_{rx} \cdot V + (DIFS + CW_{avg} \cdot T_{slot} + 3 \cdot SIFS) \cdot I_{idle} \cdot V\} \\ E_{g,d}^A &= \left( \frac{\pi_A \cdot (\tau_g - 3 \cdot T_U)}{T_{A_{avg}}} \right) \{(T_{RTS} + T_h + T_a) \cdot I_{rx} \cdot V + (T_{CTS} + T_{ACK}) \cdot I_{tx} \cdot V + (DIFS + CW_{avg} \cdot T_{slot} + 3 \cdot SIFS) \cdot I_{idle} \cdot V\} \\ E_{g,d}^C &= \left( \frac{\pi_C \cdot (\tau_g - 3 \cdot T_U)}{T_{C_{avg}}} \right) \{T_{RTS} \cdot I_{tx} \cdot V + (DIFS + CW_{avg} \cdot T_{slot}) \cdot I_{idle} \cdot V\} \\ E_{g,d} &= E_{g,d}^U + E_{g,d}^P + E_{g,d}^A + E_{g,d}^C + E_w \quad (10)\end{aligned}$$

where  $E_{g,d}^U$ ,  $E_{g,d}^P$ ,  $E_{g,d}^A$ ,  $E_{g,d}^C$ , denote the energy consumed during the transmission of a UDP packet, a TCP payload segment, a TCP acknowledgment, and during a collision respectively.  $E_w$  denotes the amount of energy consumed during wake-up i.e.  $E_w = 250 \times 10^{-6} \cdot I_{idle} \cdot V \text{ J}$ .

However, until the  $g^{th}$  geophone is polled by the WGN to begin its data transfer, it enters sleep mode for a duration as specified by the NAV metric. Note that an RTS frame transmitted by the currently scheduled geophone may not be heard by all other geophones, as they may be out of each other's range (below the energy detection threshold). In this case, the out-of-range geophone will become dependent on the CTS frame transmitted by the WGN to obtain the duration for entering sleep mode. Let  $E_{g,n}$  denote the energy consumed by the  $g^{th}$  geophone in the duration preceding its data transfer.

If the  $g'^{th}$  geophone and  $g^{th}$  geophone are within transmission range,

$$E_{g',n}^U = 3 \cdot \{(DIFS + (CW_{min} - 1)/2 \cdot T_{slot}) \cdot I_{idle} \cdot V$$

$$+T_{RTS} \cdot I_{rx} \cdot V + (T_{CTS} + T_h + T_u + T_{ACK} + 3 \cdot SIFS) \cdot I_{sl} \cdot V + E_w \} \quad (11)$$

$$E_{g',n}^P = \left( \frac{(\pi_{P_1} + \pi_{P_2}) \cdot (\tau_{g'} - 3 \cdot T_U)}{T_{P_{avg}}} \right) \{ (DIFS + CW_{avg} \cdot T_{slot}) \cdot I_{idle} \cdot V + T_{RTS} \cdot I_{rx} \cdot V + (T_{CTS} + T_h + T_p + T_{ACK} + 3 \cdot SIFS) \cdot I_{sl} \cdot V + E_w \} \quad (12)$$

else,

$$E_{g',n}^U = (3 \cdot (DIFS + (CW_{min} - 1)/2 \cdot T_{slot}) + T_{RTS} + SIFS) \cdot I_{idle} \cdot V + (2 \cdot T_{RTS} + T_{CTS}) \cdot I_{rx} \cdot V + (2 \cdot T_{CTS} + 3 \cdot (T_h + T_u + T_{ACK}) + 8 \cdot SIFS) \cdot I_{sl} \cdot V + 3 \cdot E_w \quad (13)$$

$$E_{g',n}^P = \left( \frac{(\pi_{P_1} + \pi_{P_2}) \cdot (\tau_{g'} - 3 \cdot T_U)}{T_{P_{avg}}} \right) \{ (DIFS + CW_{avg} \cdot T_{slot} + T_{RTS} + SIFS) \cdot I_{idle} \cdot V + T_{CTS} \cdot I_{rx} \cdot V + (T_h + T_p + T_{ACK} + 2 \cdot SIFS) \cdot I_{sl} \cdot V + E_w \} \quad (14)$$

The amount of energy consumed in states *A* and *C* is independent of the range between the  $g'^{th}$  and  $g^{th}$  geophones.

$$E_{g',n}^A = \left( \frac{\pi_A \cdot (\tau_{g'} - 3 \cdot T_U)}{T_{A_{avg}}} \right) \{ (DIFS + CW_{avg} \cdot T_{slot}) \cdot I_{idle} \cdot V + T_{RTS} \cdot I_{rx} \cdot V + (T_{CTS} + T_h + T_a + T_{ACK} + 3 \cdot SIFS) \cdot I_{sl} \cdot V + E_w \}$$

$$E_{g',n}^C = \pi_C \cdot (\tau_{g'} - 3 \cdot T_U) \cdot I_{idle} \cdot V$$

Summing up all contributions, an expression for the value of  $E_{g,n}$  is obtained. Note that the summation is carried out over the set  $G_g^n$ , which contains the geophones that appear before the  $g^{th}$  geophone in the schedule.

$$E_{g,n} = \sum_{g' \in G_g^n} E_{g',n}^U + E_{g',n}^P + E_{g',n}^A + E_{g',n}^C \quad (15)$$

After completing its data transfer, the  $g^{th}$  geophone enters sleep mode for the remaining duration of time taken by the subsequent geophones on the schedule, until the beginning of the next sweep. Let  $G_g^{sl}$  denote the set of geophones that appear after the  $g^{th}$  geophone in the schedule. The amount of energy consumed during this sleep period is denoted by  $E_{g,sl}$ .

$$E_{g,sl} = \sum_{g' \in G_g^{sl}} \tau_{g'} \cdot I_{sl} \cdot V \quad (16)$$

In conclusion, the total amount of energy consumed by the  $g^{th}$  geophone,  $E_g$ , using the GP scheme can be expressed as a sum of the quantities obtained from (10), (15), and (16). The average power consumption per geophone,  $P_{avg}$ , is appropriately calculated.

$$E_g = E_{g,n} + E_{g,d} + E_{g,sl} \quad (17)$$

$$= E_{g,d} + \frac{1}{2} \times \sum_{\substack{g'=1 \\ g' \neq g}}^G (E_{g',n}^U + E_{g',n}^P + E_{g',n}^A + E_{g',n}^C +$$

$$\tau_{g'} \cdot I_{sl} \cdot V) \quad (18)$$

$$P_{avg} = \frac{1}{\tau \cdot G} \times \sum_{g=1}^G E_g \quad (19)$$

The expression obtained in (18) is derived in Appendix A.

#### IV. AGTS SCHEME

In order to facilitate more efficient power saving, a geophone would ideally be aware of its own data transmission schedule, in addition to the schedules of all the other geophones in the same BSS. To provide for contention-free scheduling, an overlay-TDMA scheme can be devised such that it operates on top of the existing 802.11 DCF framework. This concept has been investigated in several works [32]–[40]. In [32], some interesting experimental results are provided for a low-power TDMA protocol over IEEE 802.11. A schedule is periodically broadcasted to all stations, and the access point has the option to dynamically modify the length of each client's time slot. Although some high-level time slot modification schemes are described, the exact nature and impact of these modifications are not analyzed. The focus is primarily on the experimental parameters for enabling TDMA over IEEE 802.11, rather than on time slot optimization. Similar functionality is implemented by the service period access scheme in [6], wherein a schedule is broadcasted by the access point and service periods are reserved for each station. However, the service periods are assumed to be of constant duration over several beacon intervals. The remaining works provide an insight into the operation of an overlay-TDMA protocol over IEEE 802.11, but either do so over an ad hoc mode of operation [33]–[38] or by imposing significant changes to the IEEE 802.11 MAC [35]–[39]. In some cases, the primary focus lies on Quality-of-Service (QoS) enhancements for 802.11 [37]–[40].

##### A. Key Features

1) *Providing Contention-Free Access:* Through the use of TDMA, contention between geophones is significantly reduced. However, incorrect synchronization or underlying frames in the buffer can cause an overlap in the transmission time of two or more geophones.

2) *Transmission Control Protocol (TCP) Fairness:* Similar to the GP scheme, the AGTS scheme allows the operation of a single TCP connection during a designated time slot, thereby circumventing the problem of TCP unfairness over 802.11.

3) *Power Saving:* The schedule is broadcasted by the WGN to all geophones, allowing for effective power saving. A geophone can enter sleep mode for the entire duration of the TDMA frame apart from its allocated time slot, similar to the approach taken in [6], [32]. A geophone can enter sleep mode before the end of its allocated time slot, if data transfer is completed prematurely. It may also enter sleep mode immediately after receiving the schedule.

4) *Open Standard*: Like the GP scheme, the AGTS scheme is also designed to require minimal modifications to the device drivers. While the GP scheme requires additional changes to expose the current status of the NAV timer to the higher layers, the AGTS scheme can operate with the already existing primitives provided by the IEEE 802.11 MAC.

5) *Adaptive Change in Time Slot Length*: Geophones at the cell-edge not only operate at higher path losses, but are also susceptible to co-channel interference. Meanwhile, geophones that are located near the WGN can transfer data more reliably. To ensure that all geophones are allocated sufficient time resources, the time slot assignment or schedule can be accordingly altered at the completion of every frame, a feature that was not analyzed in [6], [32]. New time slot lengths are obtained by scaling the time slot length in the prior frame by the ratio of the pending amount of data to the amount of data transmitted in the prior frame. The time slot length is capped at a maximum value to prevent over-allocation of time resources. Geophones that have completed data transfer are not allocated a time slot.

6) *Centralized Synchronization*: Since TDMA functionality is enforced by the upper layers, synchronization is required between the applications that are operating on the various geophones. The proposed architecture in Fig. 1 can provide more accurate synchronization using centralized schemes as compared to ad hoc schemes. Software timestamping for application synchronization can be achieved with the Timing Synchronization Function (TSF) timer [41], [42]. The TSF timer can be accessed by higher layers using the GETTSFTIME.request and GETTSFTIME.confirm primitives [20], [41].

### B. Operation

The proposed AGTS scheme relies on the use of UDP packets, much like the GP scheme, to disseminate schedule information. The UDP packets are broadcasted by the WGN, and contain information about the length of the time slot reserved for the transmission of the schedule, in addition to the length of the time slots allocated to each of the geophones in the BSS.

- 1) Initially, all geophones are allocated time slots of the same length, which is set to the maximum allowed value,  $T$ .
- 2) The WGN broadcasts UDP packets containing schedule information during a reserved time slot of duration  $\tau_{sh}$ .
- 3) During the slot reserved for schedule reception, the geophones listen to the channel for UDP broadcast packets. A geophone can enter sleep mode after securing the requisite schedule information.
- 4) Each geophone wakes up in time for data transmission using TCP, as per its allocated time slot. It remains in sleep mode for the remaining duration of the frame.
- 5) At the end of the frame, new time slot lengths are computed by the WGN. The time slot length is scaled up or down as

TABLE II: Definition of Parameters for the AGTS Scheme

Notation	Description
$T$	Maximum length of any given time slot
$f_{max}$	Maximum number of frames required for data collection
$G$	Total number of geophones within a single BSS
$D$	Total amount of data to be received from each geophone
$\tau_{sh}$	Time slot length allocated to the WGN for transmission of UDP schedule packets
$\tau_{gd}$	Guard time between adjacent time slots
$\tau_{g,f}$	Time slot length allocated to the $g^{th}$ geophone in the $f^{th}$ frame
$d_{g,f}$	Amount of data successfully transmitted by the $g^{th}$ geophone during the $f^{th}$ frame
$d_{g,f}^r$	Amount of data successfully transmitted by the $g^{th}$ geophone up to the $f^{th}$ frame

per the amount of data received in the prior frame.

$$\tau_{g,f+1} = \begin{cases} \min \left\{ \tau_{g,f} \cdot \left( \frac{D - d_{g,f}^r}{d_{g,f}} \right), T \right\} & d_{g,f}^r < D \\ 0 & d_{g,f}^r \geq D \end{cases} \quad (20)$$

$$d_{g,f}^r = \sum_{f'=1}^f d_{g,f'}$$

where  $\min\{a,b\}$  denotes the minimum of  $a$  and  $b$ . The various notations are specified in Table II.

- 6) The newly computed time slot lengths are encapsulated into a UDP packet and broadcasted by the WGN.

Steps (2-6) are repeated until data from all geophones is received by the WGN. A time slot must be long enough for the transfer of a TCP segment and its associated acknowledgement. Note that  $f$  is unbounded; frame schedules may be broadcasted by the WGN until data is received from all geophones.

A guard time is allocated to prevent overlapping between adjacent time slots. Firstly, the clock skew between geophones can lead to incorrect synchronization. Experimental results show that software timestamping using the TSF timer yields a synchronization accuracy of  $1.8 \mu s$  for a beacon interval of  $102.4 \text{ ms}$  [41]. Secondly, a duration of around  $250 \mu s$  is required to transition from sleep mode to the idle mode of operation [25], [26]. Lastly, a hardware delay of  $100 \mu s$  can also be taken into account for the guard time [34]. Hence, a suitable value for  $\tau_{gd}$  is  $350 \mu s$ .

### C. Time Analysis

An expression for the total amount of time,  $\tau$ , required for data collection using the AGTS scheme is given in (21).

$$\tau = \sum_{f=1}^{f_{max}} \left\{ \tau_{sh} + \sum_{g=1}^G (\tau_{g,f} + \tau_{gd}) \right\} \quad (21)$$

Computing the value of  $\tau_{g,f+1}$  from (20) will in turn require the value of  $d_{g,f}$  up to the  $f^{th}$  frame. The semi-Markov Process described earlier in Fig. 4 is used here for analysis. In a given time slot, collisions may occur between the allocated geophone and the WGN. Furthermore, at the boundary of

two time slots, contention may occur between two geophones and the WGN. For instance, a frame transmission initiated towards the end of a given time slot, may collide with another frame transmission in the subsequent time slot. Hence, the collision probability  $p$ , obtained from (4) and (5), can assume different values over different periods of time. To account for possible contention between geophones that have been allocated adjacent time slots, a collision domain between three stations (two geophones and the WGN) is considered in a window of length equal to  $(2 \cdot CW_{\max} \cdot T_{slot} - \tau_{gd})$ , centered at the time slot boundary. Within a given time slot of length  $\tau_{g,f}$ ,  $p$  is computed as per the time window.

$$p = \begin{cases} p_{n=3} & 0 \leq t \leq (T_w - \tau_{gd}) \\ p_{n=2} & (T_w - \tau_{gd}) < t < \tau_{g,f} - (T_w - \tau_{gd}) \\ p_{n=3} & \tau_{g,f} - (T_w - \tau_{gd}) \leq t \leq \tau_{g,f} \end{cases} \quad (22)$$

where  $T_w = CW_{\max} \cdot T_{slot}$ , and  $p_{n=i}$  denotes the collision probability computed from (4) and (5) with a total of  $i$  contending nodes.

Using the value of  $p$  and the expression derived in (6), the number of times the states  $P_1$  and  $P_2$  are entered during the time slot  $\tau_{g,f}$  can be found, following which the amount of data transmitted can be calculated.

$$d_{g,f} = \left\{ \frac{(\pi_{P_1} + \pi_{P_2}) \cdot \tau_{g,f}}{T_{P_{avg}}} \right\} \cdot E(P) \quad (23)$$

The value of  $\tau_{g,f+1}$  can then be found from (20), making this analysis an iterative procedure.

#### D. Power Consumption Analysis

An analysis is extended to the average power consumption of the geophones. The energy consumed during data transfer over a period of  $\tau_{g,f}$  can be denoted by  $E_{g,f}^d$ , and calculated as a sum of the energies consumed in each of the states described in Fig. 4.

$$\begin{aligned} E_{g,f}^P &= \left( \frac{(\pi_{P_1} + \pi_{P_2}) \cdot \tau_{g,f}}{T_{P_{avg}}} \right) \{(T_{RTS} + T_h + T_p) \cdot I_{tx} \cdot V + (T_{CTS} + T_{ACK}) \cdot I_{rx} \cdot V + (DIFS + CW_{avg} \cdot T_{slot} + 3 \cdot SIFS) \cdot I_{idle} \cdot V\} \\ E_{g,f}^A &= \left( \frac{\pi_A \cdot \tau_{g,f}}{T_{A_{avg}}} \right) \{(T_{RTS} + T_h + T_a) \cdot I_{rx} \cdot V + (T_{CTS} + T_{ACK}) \cdot I_{tx} \cdot V + (DIFS + CW_{avg} \cdot T_{slot} + 3 \cdot SIFS) \cdot I_{idle} \cdot V\} \\ E_{g,f}^C &= \left( \frac{\pi_C \cdot \tau_{g,f}}{T_{C_{avg}}} \right) \{T_{RTS} \cdot I_{tx} \cdot V + (DIFS + CW_{avg} \cdot T_{slot}) \cdot I_{idle} \cdot V\} \\ E_{g,f}^d &= E_{g,f}^P + E_{g,f}^A + E_{g,f}^C + 2 \cdot E_w \end{aligned} \quad (24)$$

where  $E_{g,f}^P$  denotes the energy consumed in the  $P_1$  and  $P_2$  states,  $E_{g,f}^A$  in the  $A$  state, and  $E_{g,f}^C$  in the  $C$  state. The factor of  $2 \cdot E_w$  in (24) accounts for the energy consumed during wake-up; initially at the beginning of the frame, and subsequently at the beginning of the allocated time slot. Apart from the energy consumed during the allocated time slot, an

additional amount of energy  $E_{g,f}^{sl}$  is consumed while in sleep mode for the remaining duration of the frame. Some amount of energy,  $E_{g,f}^{sh}$ , is consumed during the time slot reserved for schedule reception from the WGN.

$$E_{g,f}^{sl} = \sum_{\substack{g'=1 \\ g' \neq g}}^G (\tau_{g',f} + \tau_{gd}) \cdot I_{sl} \cdot V$$

Summing up the individual contributions results in an expression for the total energy consumed by the  $g^{th}$  geophone during the  $f^{th}$  frame,  $E_{g,f}$ . The average power consumption per geophone  $P_{avg}$  is then accordingly found.

$$E_{g,f} = E_{g,f}^d + E_{g,f}^{sl} + E_{g,f}^{sh} \quad (25)$$

$$P_{avg} = \frac{1}{\tau \cdot G} \times \sum_{f=1}^{f_{max}} \sum_{g=1}^G E_{g,f} \quad (26)$$

#### V. LISTEN INTERVAL ACQUISITION

While some implementations of seismic acquisition may require data to be transmitted only after the listen interval, so as to perform some pre-processing of the data locally at the geophones, other implementations would begin acquiring data during the listen interval, and perform all the processing of the data at the DCC or a remote server. In this section, a data collection scheme that can be applied during the listen interval is discussed.

The aforementioned GP and AGTS schemes rely on the amount of data which is buffered and readily available for transfer from a geophone. This is determined by the value of  $D$ , which is simply the product of the data generation rate at the geophone  $R_l$ , and the duration of the listen interval  $T_{LI}$ . However, during the listen interval, data is recorded ‘on-the-go’ and a suitable value for  $D$  cannot be determined so as to employ the GP or AGTS scheme. This motivates the use of a single TDMA frame for the entirety of the listen interval, wherein each geophone is allocated a time slot for data transfer. In order to conserve power, geophones can enter sleep mode for the duration outside their allocated time slot. A guaranteed time slot during the listen interval also ensures that the quality control information  $Q$  is transferred every sweep, where  $Q$  is typically around 1-10 bytes in size [4]. At the end of the listen interval, the value of  $D$  designated to each geophone can be altered by the WGN by simply subtracting the amount of information received from the respective geophone during the listen interval, following which the GP or AGTS scheme can be applied for the remaining period of data acquisition.

The problem of determining an optimal value for the time slots to be allocated to the geophones during the listen interval is investigated here. An optimal time slot assignment strategy can be determined so as to maximize the total amount of data received by the WGN during the listen interval. While the seismic data is generated by the geophones at a rate  $R_l$ , on the order of several Kbps, any data that has already been buffered can be queued for transmission at a much higher rate, say  $R_b$ , on the order of several Mbps. In our scenario,  $R_b$  would

typically be rate-limited by the maximum achievable transfer rates over the 802.11af links.

Consider a total of  $G$  geophones being serviced by a single WGN, where the amount of data received at the WGN from the  $g^{th}$  geophone is  $d_g$ , the corresponding length of the time slot allocated to it is  $\tau_g$ , and the duration of the guard time allocated between time slots is  $\tau_{gd}$ . For ease of analysis, let us assume that the geophones are allocated time slots in increasing order. In this scenario, the first geophone would simply transfer data at rate  $R_l$  over a duration of  $\tau_1$ . Meanwhile, the second geophone would have buffered data during  $(\tau_1 + \tau_{gd})$  which can now be transmitted at the higher rate  $R_b$ . This effect ripples along the geophones for the entire duration of the listen interval. An expression for  $d_g$  can be formulated accordingly.

$$d_g = \left[ Q + R_l \cdot \sum_{g'=1}^{g-1} (\tau_{g'} + \tau_{gd}) \right] + \\ R_l \cdot \left[ \tau_g - \frac{R_l}{R_b} \cdot \left\{ \frac{Q}{R_l} + \sum_{g'=1}^{g-1} (\tau_{g'} + \tau_{gd}) \right\} \right] \quad (27)$$

$$= \left[ Q - R_l \cdot \tau_{gd} + R_l \cdot \sum_{g'=1}^g (\tau_{g'} + \tau_{gd}) \right] - \\ \frac{R_l^2}{R_b} \cdot \left[ \frac{Q}{R_l} + \sum_{g'=1}^{g-1} (\tau_{g'} + \tau_{gd}) \right] \quad (28)$$

The first term in (27) accounts for the data buffered during the time slots leading up to the  $g^{th}$  geophone, while the second term accounts for the seismic data that is recorded and transmitted during  $\tau_g$ . By maximizing the sum of the data received from all the geophones at the WGN, the optimal time slot values ( $\hat{\tau}_1, \hat{\tau}_2, \dots, \hat{\tau}_G$ ) can be computed. A linear optimization problem is set up through (29)-(32), with the constant terms (independent of the time slots) in (28) not being considered in the objective function in (30).

$$(\hat{\tau}_1, \hat{\tau}_2, \dots, \hat{\tau}_G) = \arg \max_{\tau_1, \tau_2, \dots, \tau_G} \sum_{g=1}^G d_g \quad (29)$$

$$= \arg \max_{\tau_1, \tau_2, \dots, \tau_G} \left\{ R_l \cdot \sum_{g=1}^G \sum_{g'=1}^g \tau_{g'} - \frac{R_l^2}{R_b} \cdot \sum_{g=1}^G \sum_{g'=1}^{g-1} \tau_{g'} \right\} \quad (30)$$

$$\tau_g \geq \frac{R_l}{R_b} \cdot \left\{ \frac{Q}{R_l} + \sum_{g'=1}^{g-1} (\tau_{g'} + \tau_{gd}) \right\} \quad (31)$$

$$T_{LI} = \sum_{g=1}^G (\tau_g + \tau_{gd}) \quad (32)$$

Constraint (31) is formulated by imposing a minimum value for a time slot such that the buffered seismic data and the quality control information is transferred. Constraint (32) ensures that the sum of all time slots, along with the corresponding guard times, is equal to  $T_{LI}$ .

TABLE III: Simulation Parameters

Parameter	Value	Parameter	Value
Operating Frequency	470 MHz	TCP Maximum Segment Size	2200 bytes
Bandwidth	8 MHz	Beacon Interval	102.4 ms
Listen Interval	6 s	CFP Duration	80 ms
Sweep Length	8 s	SIFS	90 $\mu$ s
Move-up Interval	8 s	PIFS	110 $\mu$ s
Data Generation Rate	144 kbps	DIFS	130 $\mu$ s
WGN Antenna Height	3 m	RTS/CTS Signalling	Enabled
Geophone Antenna Height	1 m	Short Guard Interval	Enabled
Max Transmit Power	20 dBm	Supply Voltage (V)	3 V
Receiver Sensitivity	-87 dBm	Current in transmit mode ( $I_{tx}$ )	380 mA
CCA Sensitivity	-87 dBm	Current in receive mode ( $I_{rx}$ )	313 mA
Noise Figure	6 dB	Current in idle mode ( $I_{idle}$ )	273 mA
Max PHY Data Rate	35.6 Mbps	Current in sleep mode ( $I_{sl}$ )	33 mA

## VI. PERFORMANCE EVALUATION

The ns-3 simulator is used for evaluation [43]. The simulation parameters are listed in Table III. Propagation loss measurements that were made in Ultra-High Frequency (UHF) bands for antenna heights between 0.3 m and 1.5 m show a good agreement with the two-ray propagation model [44]. Regarding the power consumption parameters, experimental studies using IEEE 802.11af chipsets for specific scenarios (such as the transmit, receive, idle, and sleep modes of operation) have not been reported in literature. In order to gain a perspective on the relative performance comparison between the various channel access schemes discussed in this work, we assume the power consumption parameters to be those of an IEEE 802.11n chipset [45].

### A. Simulation Results

Performance is evaluated at the WGN having the largest BSS across the seismic survey area. A comparison between the analysis and simulation results is presented in Fig. 5, with  $K = 7$  and  $CW_{min} = 16$ . The value of  $G$  is also shown for each corresponding value of  $R$ . Listen interval acquisition is not considered, since we are interested solely in the analysis of the GP and AGTS schemes in this section.

The time analysis of the GP scheme closely follows the simulation result in Fig. 5a, where the deviation arises from the assumption of perfectly saturated traffic, which in turn leads to an overestimation of the value of  $p$ . In Fig. 5b, the deviation can also be attributed to the fact that the analytical model considers an average across all the possible permutations of the schedule, whereas it would be infeasible to conduct such numerous simulations. For instance, a WGN cell radius of 400 m would amount to a total of approximately  $1.24 \times 10^{142}$  number of possible schedules. Results for the AGTS scheme are shown in Fig. 5c-5d. For a given value of  $R$ ,  $T$  is chosen such that the least value of  $\tau$  is obtained. While the time analysis closely follows the simulation result in Fig. 5c, the deviation in the power consumption is much smaller in Fig. 5d.

On inspecting Fig. 5a and 5c, there is an exponential increase in the amount of time taken by the DCF scheme with an increase in the number of geophones per cell, which is

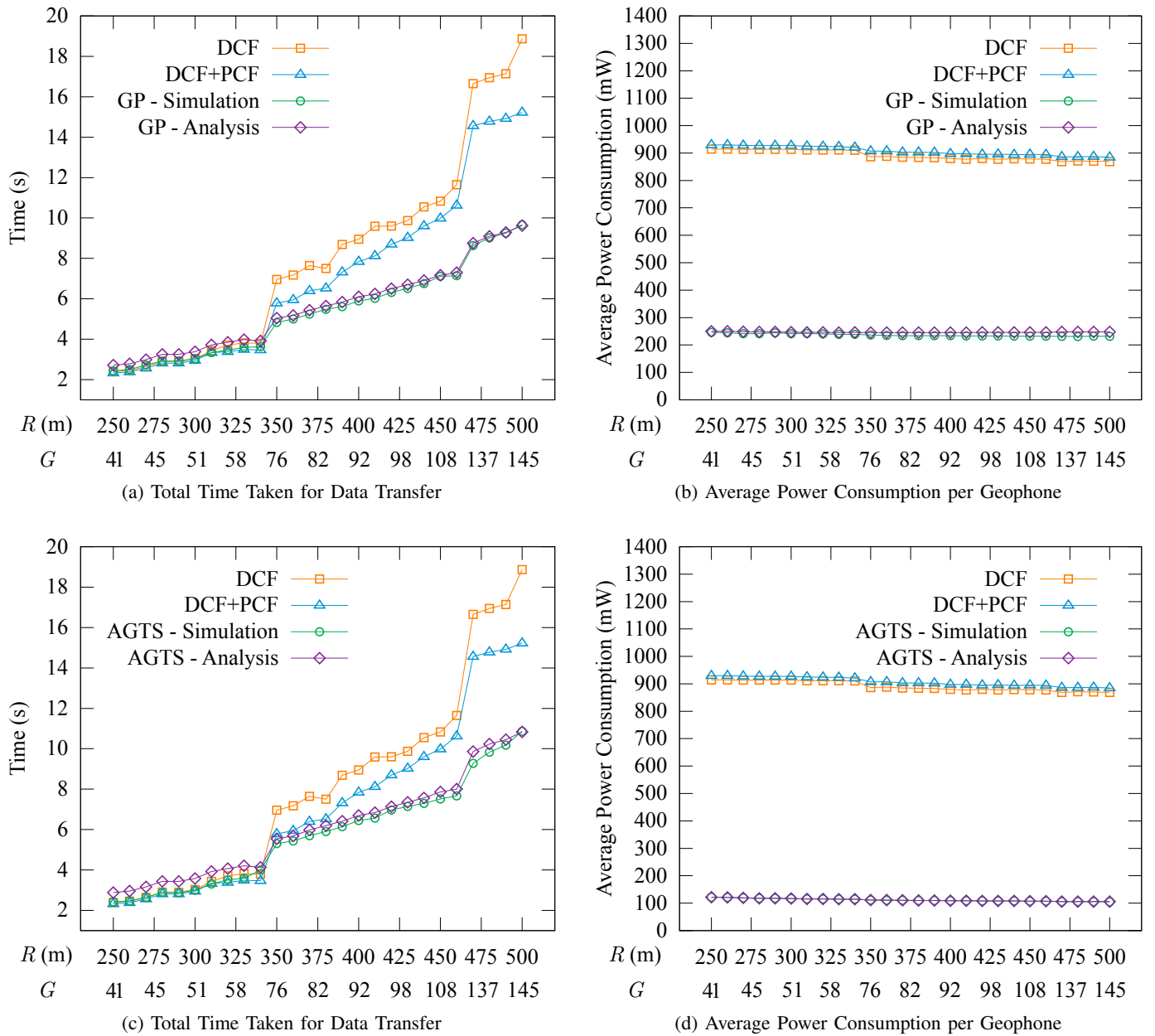


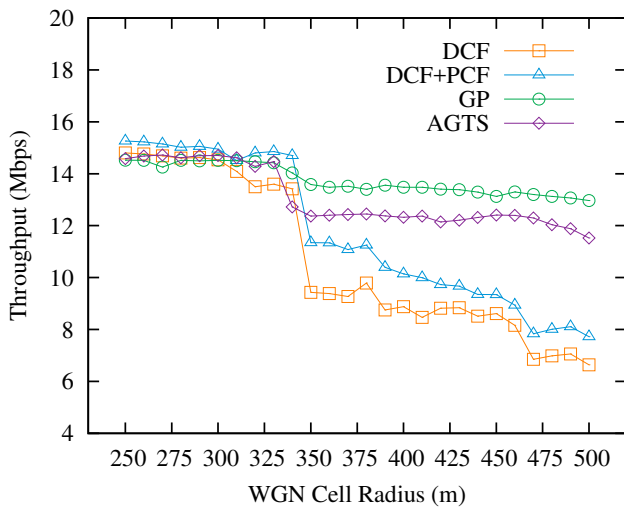
Fig. 5: Performance Evaluation: Analysis vs Simulation

expected. Although the PCF channel access scheme performs well for small cell radii, it does not scale with the number of geophones. As the cell radius increases, the polling list becomes larger, and the WGN must poll several ‘empty’ geophones before interacting with subsequent geophones that have data to transmit. Furthermore, the geophones experience severe contention during the CP. The GP scheme performs better than the AGTS scheme due to the fact that every geophone is allowed to transfer data for an unbounded amount of time. Meanwhile, time resources are under/over allocated to the geophones in the AGTS scheme. For instance, all the geophones are allocated time slots of equal length in the first frame.

From Fig. 5b and 5d, it can be inferred that about 73.5% and 87.4% of power is conserved by the GP and AGTS

schemes respectively, as compared to the DCF scheme. Such effective power saving has been achieved by exploiting the deterministic and delay-tolerant nature of the traffic generated in geophone networks. The AGTS scheme is able to achieve better power saving with the aid of a global schedule known to all geophones. On the other hand, in the GP scheme, the geophones are required to cycle between the sleep and idle modes of operation for every update of the NAV counter.

Additional metrics for performance evaluation are plotted in Fig. 6. In Fig. 6a, the throughput at the WGN is compared for the various data collection schemes. As the cell radius increases, the number of geophones per WGN increases, consequently resulting in reduced throughput. The uniformity in the power consumption can be measured by the standard deviation ( $\sigma$ ), which is plotted in Fig. 6b. Overall,  $\sigma$  is



(a) Throughput at the WGN

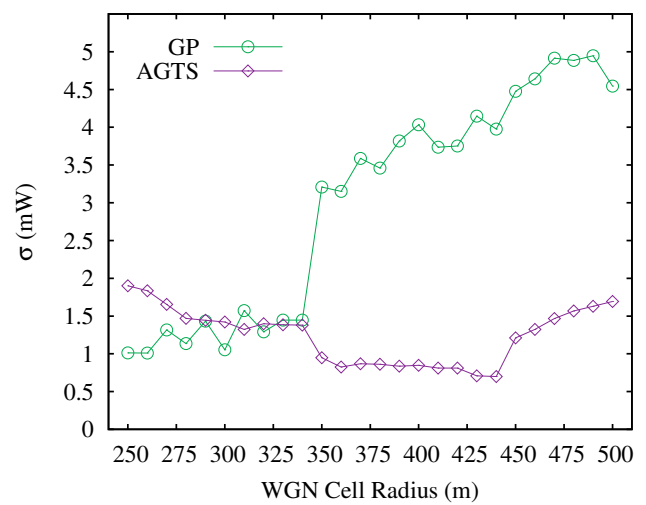
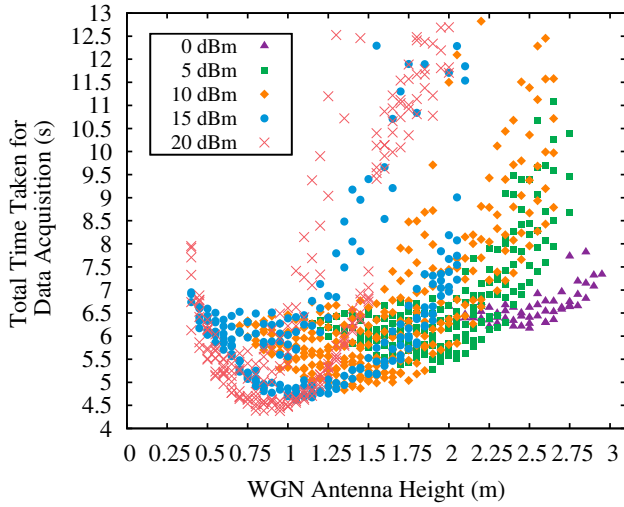
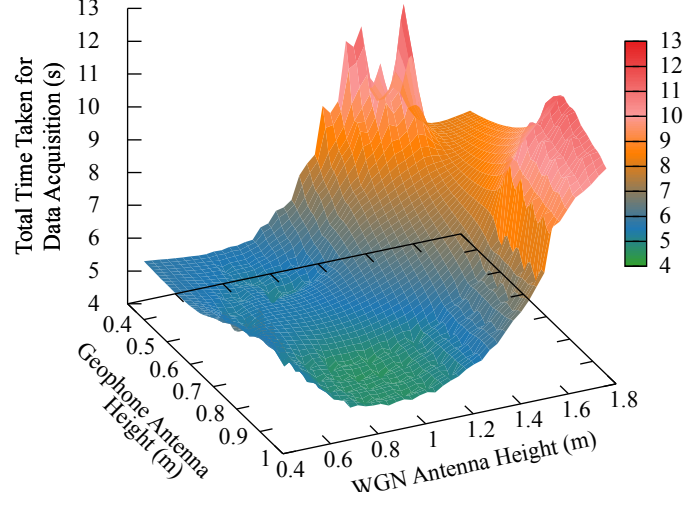
(b) Standard Deviation ( $\sigma$ ) of the Average Power Consumption

Fig. 6: Performance Evaluation: Throughput and Uniformity of Power Consumption



(a) Scatter Plot of Acquisition Times



(b) Variation in the Geophone and WGN Antenna Heights

Fig. 7: Variation of Antenna Heights and Transmit Power to combat Co-Channel Interference

minimal, not exceeding 2 mW and 5 mW for the AGTS and GP schemes respectively. In the GP scheme, the increasing trend of  $\sigma$  with  $R$  arises from the fact that for an increasing value of  $R$ , a greater number of geophones would be out of range from one another, leading to a disparity in the manner in which  $E_{g,n}$  is computed using (11)-(14).

### B. Impact of Co-Channel Interference

Frequency reuse is inherently associated with co-channel interference (CCI), that can strongly impact the overall performance of the system. Tall antennas for the WGN can result in a severely interference-limited system, wherein a large frequency reuse factor is required to maintain an acceptable level of co-channel interference into neighboring co-channel cells. Moreover, shorter antennas are more desirable from a logistics perspective and to ensure robustness to high wind

speeds. Consequently, the antenna heights for the WGN and the geophones can be capped at 3 m and 1 m respectively.

A scatter plot of the total acquisition times, for a WGN cell radius of 250 m employing the GP scheme with 8 MHz channels, is provided in Fig. 7a as a function of the WGN antenna height and the transmit power. A 4-cell reuse pattern is considered in this analysis, since a 3-cell pattern is severely interference-limited and a 7-cell pattern would require an excessive number of available channels. A key observation to be noted is that the acquisition time decreases with increasing transmit power, with a transmit power of 20 dBm performing the best. This suggests that higher transmit powers produce a higher SINR, resulting in lower acquisition times by operating at higher data rates more reliably. Additionally, for a given transmit power, the most suitable WGN antenna height that yields a minimum acquisition time decreases with increasing

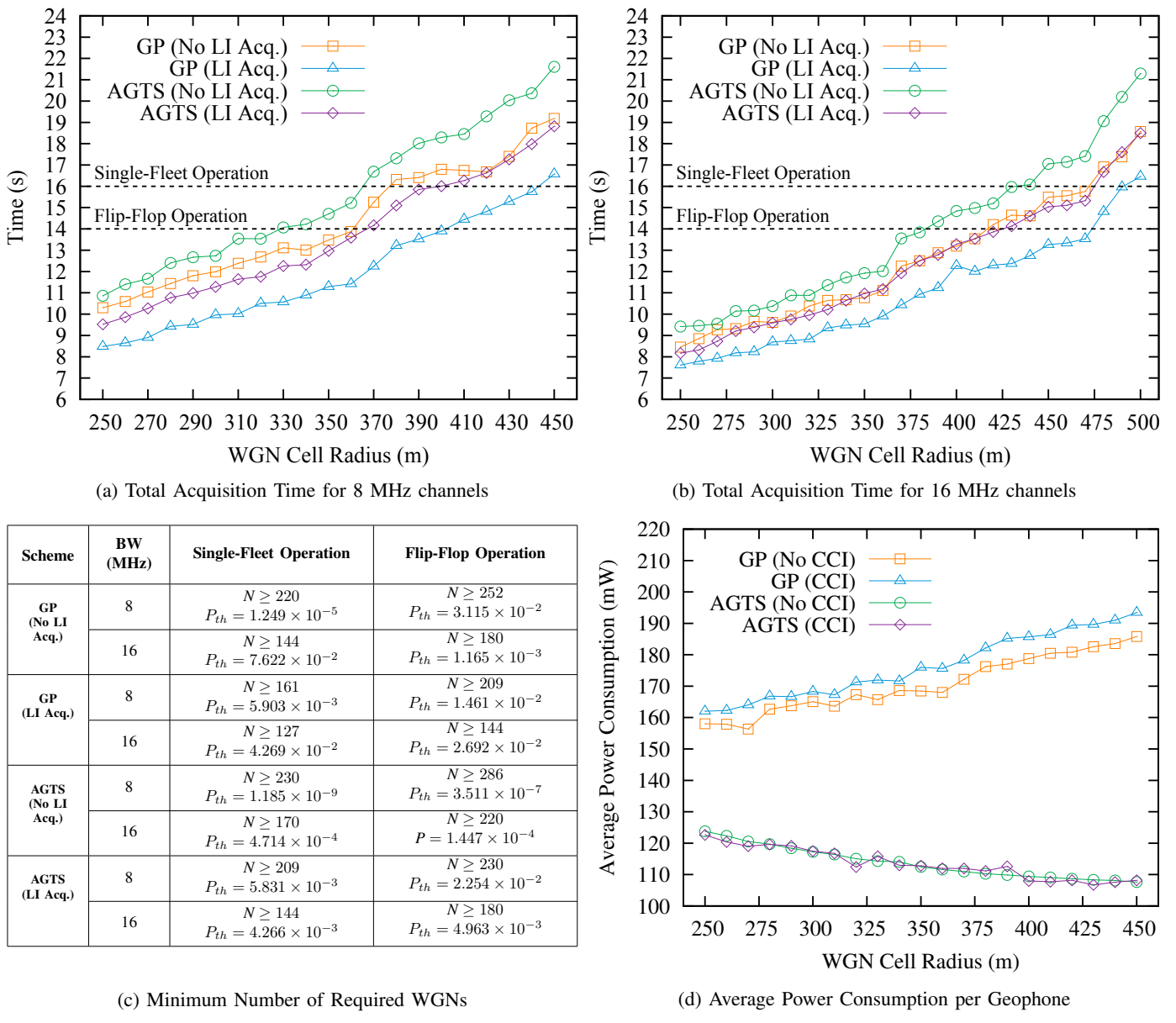


Fig. 8: Performance Evaluation in the presence of Co-Channel Interference

transmit power. This arises from the fact that a higher transmit power would encroach more easily upon the neighboring co-channel cells, consequently requiring shorter antenna heights to mitigate this effect. The influence of the geophone antenna heights is depicted in Fig. 7b, given a transmit power of 20 dBm. It can be seen that minimal acquisition time is achieved when the geophone antenna height is in the range of 0.8–1 m, and the WGN antenna height is in the range of 0.8–1.1 m. For WGN antenna heights exceeding 1.5 m, the performance deteriorates rapidly and the acquisition time is nearly tripled, as compared to the minimal value. Hence, an antenna height in the range of 0.8–1 m and 0.8–1.1 m is most suitable for the geophones and the WGNs respectively, along with a transmit power of 20 dBm, under the assumed flat Earth propagation model.

The GP and AGTS schemes are now evaluated for the first tier of co-channel cells. As per the acquisition parameters

described in Table III, the resultant thresholds for flip-flop and single-fleet modes of operation are 14 s and 16 s respectively. Listen interval acquisition is considered here, wherein the optimal time slot values are computed by numerically solving the objective function in (30).  $R_l$  is taken to be 144 kbps, while in the case of  $R_b$ , a modest assumption of 5 Mbps and 10 Mbps is made for 8 MHz and 16 MHz channels respectively. The values assumed for  $R_b$  match closely with the findings observed in simulation.

Results for the total acquisition time and average power consumption are obtained in Fig. 8, wherein the phrase ‘listen interval acquisition’ has been shortened to ‘LI Acq.’ In Fig. 8a, the total acquisition time using 8 MHz channels is plotted, where it can be inferred that the GP scheme performs better than the AGTS scheme under the impact of CCI as well. Acquiring data during the listen interval presents considerable gains for both schemes. Similar observations can be made in

Fig. 8b for 16 MHz channels, where the overall performance is much improved, at the cost of an additional 4 channels. The minimum required number of WGNs ( $N$ ) can be obtained as a function of the WGN cell radius using (1). By modelling the results to be Gaussian distributed, the probability that the total acquisition time exceeds the threshold ( $P_{th}$ ) can be found [19]. These quantities are listed in Fig. 8c.

The impact of CCI on the average power consumption can be seen in Fig. 8d, after taking listen interval acquisition into account. There is a marginal increase in the power consumption for the GP scheme in the presence of CCI. This can be attributed to the fact that a primary feature of the GP scheme's power saving strategy is to utilize the NAV counter for determining a duration for operating in sleep mode. Under the impact of CCI, an increased number of collisions are witnessed due to transmissions from the neighboring co-channel cells, thereby causing a decline in power saving performance. On the other hand, the AGTS scheme is relatively unaffected by CCI since the power saving performance is determined by a broadcasted schedule with stringent limits on the time slot lengths.

## VII. CONCLUSION

A wireless geophone network based on the IEEE 802.11af standard has been described, that can operate with minimal amount of standards-compliant hardware in a spectrally-efficient manner. Although the default channel access schemes provided by the standard are not ideal, the total time required for data collection and the average power consumption of the geophones can be reduced by implementing functionality through the GP and AGTS schemes. While the GP scheme performs best in terms of acquisition time, it is not as power-efficient as the AGTS scheme. On the other hand, the AGTS scheme is the best for power saving, but at the cost of an increased amount of time for data acquisition.

An important feature of the proposed architecture is its scalability. Given that flip-flop operations are employed and the GP scheme is operated over four 802.11af channels, a total of 209 WGNs is sufficient to map an area as large as 72 km<sup>2</sup>, after accounting for co-channel interference. This number is further reduced to 144 WGNs when eight 802.11af channels are available, which is likely the case in remote areas, to operate with 16 MHz of bandwidth. At the expense of a higher number of WGNs, more power saving can be obtained by utilizing the AGTS scheme. Thus, a reduction in the power consumption and the required amount of hardware for data acquisition translates to a reduced cost in terms of the equipment weight, transportation, and manpower, and also offers a greener alternative to cable-based systems. Future work will involve the design of data communication protocols from the WGNs to the DCC in an energy-efficient manner.

## APPENDIX A

Let the probability that the  $g^{th}$  geophone lies at the  $i^{th}$  position in the schedule be denoted by  $\alpha$ . For  $i = 1$ ,  $\alpha = 1/G$

as there are a total of  $G$  geophones that can occupy the first position in the schedule. For  $i \geq 2$ ,

$$\begin{aligned}\alpha &= \left\{ \prod_{j=0}^{i-2} \left(1 - \frac{1}{G-j}\right) \right\} \left(\frac{1}{G-i+1}\right) \\ &= \left(\frac{G-1}{G}\right) \left(\frac{G-2}{G-1}\right) \left(\frac{G-3}{G-2}\right) \dots \\ &\quad \dots \left(\frac{G-i+2}{G-i+1}\right) \left(\frac{G-i+1}{G-i+2}\right) \left(\frac{1}{G-i+1}\right) \\ &= \frac{1}{G}\end{aligned}$$

Hence,  $\alpha = 1/G$  irrespective of the position in the schedule. This also reaffirms the uniform distribution of geophones in the schedule.

In equation (15), energy is summed over all the geophones belonging to the set  $G_g^n$ . Let  $\beta$  be the probability that the  $g^{th}$  geophone appears before the  $g^{th}$  geophone in the schedule, i.e.  $\beta = \Pr\{g' \in G_g^n\}$ .

$$\begin{aligned}\beta &= \sum_{i=1}^G (\Pr\{g^{th} \text{ geophone appears before the position } i\} \\ &\quad \times \Pr\{g^{th} \text{ geophone lies in position } i\}) \\ &= \sum_{i=1}^G \left(\frac{i-1}{G-1}\right) \times \alpha \\ &= \frac{1}{G(G-1)} \left(\frac{G(G+1)}{2} - G\right) \\ &= \frac{1}{2}\end{aligned}$$

Equation (15) can be rewritten accordingly.

$$\begin{aligned}E_{g,n} &= \sum_{g' \in G_g^n} E_{g',n}^U + E_{g',n}^P + E_{g',n}^A + E_{g',n}^C \\ &= \sum_{\substack{g'=1 \\ g' \neq g}}^G \beta \cdot (E_{g',n}^U + E_{g',n}^P + E_{g',n}^A + E_{g',n}^C) \\ &= \frac{1}{2} \times \sum_{\substack{g'=1 \\ g' \neq g}}^G E_{g',n}^U + E_{g',n}^P + E_{g',n}^A + E_{g',n}^C \quad (33)\end{aligned}$$

Since  $G_g^{sl}$  and  $G_g^n$  are mutually exclusive sets,  $\Pr\{g' \in G_g^{sl}\} = 1 - \Pr\{g' \in G_g^n\} = 1 - \beta$ . Using this result, equation (16) can be rewritten.

$$\begin{aligned}E_{g,sl} &= \sum_{g' \in G_g^{sl}} \tau_{g'} \cdot I_{sl} \cdot V \\ &= \sum_{\substack{g'=1 \\ g' \neq g}}^G (1 - \beta) \cdot (\tau_{g'} \cdot I_{sl} \cdot V) \\ &= \frac{1}{2} \times \sum_{\substack{g'=1 \\ g' \neq g}}^G \tau_{g'} \cdot I_{sl} \cdot V \quad (34)\end{aligned}$$

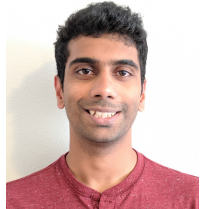
The above results are used to evaluate the total energy consumed by the  $g^{th}$  geophone,  $E_g$ , in (18). Furthermore, it can

be inferred that  $\forall g$ ,  $E_g$  is independent of the nature of  $G_g^n$  or  $G_g^{sl}$ , i.e. the order that the geophones are polled in. Hence, statistically, a uniform power consumption is achieved across all the geophones over several sweeps.

## REFERENCES

- [1] G. Vermeer, *3D Seismic Survey Design*, 2nd ed. Society of Exploration Geophysicists, 2012.
- [2] A. Cordinen, M. Galbraith, and J. Peirce, *Planning Land 3-D Seismic Surveys*. Society of Exploration Geophysicists, 2000.
- [3] S. Savazzi and U. Spagnolini, "Wireless geophone networks for high-density land acquisition: Technologies and future potential," *The Leading Edge*, vol. 27, no. 7, pp. 882–886, 2008.
- [4] S. Savazzi, U. Spagnolini, L. Goratti, D. Molteni, M. Latva-aho, and M. Nicoli, "Ultra-wide band sensor networks in oil and gas explorations," *IEEE Communications Magazine*, vol. 51, no. 4, pp. 150–160, April 2013.
- [5] S. Savazzi, D. Molteni, and U. Spagnolini, "Energy-aware compress and forward systems for wireless monitoring of time-varying fields," in *21st Annual IEEE International Symposium on Personal, Indoor and Mobile Radio Communications*, Sep. 2010, pp. 1384–1389.
- [6] V. A. Reddy, G. L. Stüber, and S. I. Al-Dharrab, "High-Speed Seismic Data Acquisition Over mm-Wave Channels," in *2018 IEEE 88th Vehicular Technology Conference (VTC-Fall)*, Aug 2018, pp. 1–5.
- [7] D. B. Crice, "Systems and methods for seismic data acquisition," *U.S. Patent 9,291,732*, March 2016.
- [8] C. W. Chen and Y. Wang, "Chain-Type Wireless Sensor Network for Monitoring Long Range Infrastructures: Architecture and Protocols," *International Journal of Distributed Sensor Networks*, vol. 4, no. 4, pp. 287–314, 2008.
- [9] K. Elder, A. T. Prokop, and S. Kooper, "Wireless seismic system with phased antenna array," *U.S. Patent 10,241,22*, March 2019.
- [10] H. Jamali-Rad and X. Campman, "Internet of Things-based Wireless Networking for Seismic Applications," *Geophysical Prospecting*, vol. 66, no. 4, pp. 833–853, 2018.
- [11] V. A. Reddy, G. L. Stüber, and S. I. Al-Dharrab, "Energy Efficient Network Architecture for Seismic Data Acquisition via Wireless Geophones," in *2018 IEEE International Conference on Communications (ICC)*, May 2018, pp. 1–5.
- [12] "IEEE Standard for Local and metropolitan area networks - Part 11: Wireless LAN medium access control (MAC) and physical layer (PHY) specifications - Amendment 5: Adoption of IEEE Std 802.11af-2014," pp. 1–204, Aug 2015.
- [13] A. B. Flores, R. E. Guerra, E. W. Knightly, P. Ecclesine, and S. Pandey, "IEEE 802.11af: a standard for TV white space spectrum sharing," *IEEE Communications Magazine*, vol. 51, no. 10, pp. 92–100, October 2013.
- [14] "IEEE Standard for Local and metropolitan area networks - Part 15.4: Low-Rate Wireless Personal Area Networks (LR-WPANs) - Amendment 6: TV White Space Between 54 MHz and 862 MHz Physical Layer," pp. 1–118, April 2014.
- [15] J. S. Urn, S. H. Hwang, and B. J. Jeong, "A comparison of PHY layer on the Ecma-392 and IEEE 802.11af standards," in *2012 7th International ICST Conference on Cognitive Radio Oriented Wireless Networks and Communications (CROWNCOM)*, June 2012, pp. 313–319.
- [16] A. N. Mody and G. Chouinard, "Overview of IEEE 802.22 Standard," June 2010. [Online]. Available: <http://www.ieee802.org/22/Technology/22-10-0073-03-0000-802-22-overview-and-core-technologies.pdf>
- [17] C. Bagaini, T. Bunting, A. El-Emam, and A. Laake, "Land Seismic Techniques for High-Quality Data," *Oilfield Review*, vol. 22, no. 2, 2010.
- [18] D. Mougenot, "Land seismic: needs and answers," *First Break*, vol. 22, no. 2, February 2004.
- [19] G. L. Stüber, *Principles of Mobile Communication*, 4th ed. Springer International Publishing, 2017.
- [20] "IEEE Standard for Local and metropolitan area networks - Part 11: Wireless LAN Medium Access Control (MAC) and Physical Layer (PHY) Specifications," pp. 1–3534, Dec 2016.
- [21] K. Leung and V. O. K. Li, "Transmission control protocol (TCP) in wireless networks: issues, approaches, and challenges," *IEEE Communications Surveys Tutorials*, vol. 8, no. 4, pp. 64–79, 2006.
- [22] N. Blefari-Melazzi, A. Detti, I. Habib, A. Ordine, and S. Salsano, "TCP Fairness Issues in IEEE 802.11 Networks: Problem Analysis and Solutions Based on Rate Control," *IEEE Transactions on Wireless Communications*, vol. 6, no. 4, pp. 1346–1355, April 2007.
- [23] K. Omori, Y. Tanigawa, and H. Tode, "A study on power saving using RTS/CTS handshake and burst transmission in wireless LAN," in *2015 10th Asia-Pacific Symposium on Information and Telecommunication Technologies (APSITT)*, Aug 2015, pp. 1–3.
- [24] A. Azcorra, I. Ucar, F. Gringoli, A. Banchs, and P. Serrano, "Nap: Practical micro-sleeps for 802.11 WLANs," *Computer Communications*, vol. 110, pp. 175 – 186, 2017.
- [25] R. Palacios, F. Granelli, D. Klazovich, L. Alonso, and J. Alonso-Zarate, "An energy efficient distributed coordination function using bidirectional transmissions and sleep periods for IEEE 802.11 WLANs," in *2013 IEEE Global Communications Conference (GLOBECOM)*, Dec 2013, pp. 1619–1625.
- [26] P. Havinga and G. Smit, "Energy-efficient TDMA medium access control protocol scheduling," in *Proceedings 1st Asian International Mobile Computing Conference (AMOC 2000)*, 11 2000, pp. 1–10.
- [27] S. Ross, *Introduction to Probability Models (Eleventh Edition)*. Academic Press, 2014.
- [28] R. Braden, "Requirements for Internet Hosts - Communication Layers," Internet Requests for Comments, RFC Editor, STD 3, October 1989. [Online]. Available: <http://www.rfc-editor.org/rfc/rfc1122.txt>
- [29] G. Bianchi, "Performance analysis of the IEEE 802.11 distributed coordination function," *IEEE Journal on Selected Areas in Communications*, vol. 18, no. 3, pp. 535–547, March 2000.
- [30] S. Gopal, S. Paul, and D. Raychaudhuri, "Investigation of the TCP simultaneous-send problem in 802.11 wireless local area networks," in *2005 IEEE International Conference on Communications (ICC)*, vol. 5, May 2005.
- [31] H. L. Vu and T. Sakurai, "Collision probability in saturated IEEE 802.11 networks," in *In Australian Telecommunication Networks and Applications Conference*, 2006.
- [32] J. Snow, W. Feng, and W. Feng, "Implementing a low power TDMA protocol over 802.11," in *IEEE Wireless Communications and Networking Conference*, 2005, vol. 1, March 2005, pp. 75–80 Vol. 1.
- [33] A. Rao and I. Stoica, "An Overlay MAC Layer for 802.11 Networks," in *Proceedings of the 3rd International Conference on Mobile Systems, Applications, and Services*, ser. MobiSys '05. New York, NY, USA: ACM, 2005, pp. 135–148.
- [34] P. Djukic and P. Mohapatra, "Soft-TDMAC: A Software TDMA-Based MAC over Commodity 802.11 Hardware," in *IEEE INFOCOM 2009*, April 2009, pp. 1836–1844.
- [35] B. Raman and K. Chebolu, "Design and Evaluation of a New MAC Protocol for Long-distance 802.11 Mesh Networks," in *Proceedings of the 11th Annual International Conference on Mobile Computing and Networking*, ser. MobiCom '05. New York, NY, USA: ACM, 2005, pp. 156–169.
- [36] R. Patra, S. Nedevschi, S. Surana, A. Sheth, L. Subramanian, and E. Brewer, "WILDNet: Design and Implementation of High Performance WiFi Based Long Distance Networks," in *4th USENIX Symposium on Networked Systems Design & Implementation (NSDI 07)*. Cambridge, MA: USENIX Association, 2007.
- [37] Y. Cheng, D. Yang, and H. Zhou, "Det-WiFi: A Multihop TDMA MAC Implementation for Industrial Deterministic Applications Based on Commodity 802.11 Hardware," *Wireless Communications and Mobile Computing*, p. 10, 2017.
- [38] G. Liaw and Y. Yeh, "A TDMA Medium Access Control Mechanism for IEEE 802.11-Based Wireless Networks," in *2011 Fifth International Conference on Genetic and Evolutionary Computing*, Aug 2011, pp. 61–64.
- [39] R. Costa, P. Portugal, F. Vasques, and R. Moraes, "A TDMA-based mechanism for real-time communication in IEEE 802.11e networks," in *2010 IEEE 15th Conference on Emerging Technologies Factory Automation (ETFA 2010)*, Sept 2010, pp. 1–9.
- [40] Y. Wei, Q. Leng, S. Han, A. K. Mok, W. Zhang, and M. Tomizuka, "RT-WiFi: Real-Time High-Speed Communication Protocol for Wireless Cyber-Physical Control Applications," in *2013 IEEE 34th Real-Time Systems Symposium*, Dec 2013, pp. 140–149.
- [41] A. Mahmood, R. Exel, H. Trsek, and T. Sauter, "Clock Synchronization Over IEEE 802.11 - A Survey of Methodologies and Protocols," *IEEE Transactions on Industrial Informatics*, vol. 13, no. 2, pp. 907–922, April 2017.
- [42] A. Mahmood, R. Exel, and T. Sauter, "Impact of hard-and software timestamping on clock synchronization performance over IEEE 802.11," in *2014 10th IEEE Workshop on Factory Communication Systems (WFCS 2014)*, May 2014, pp. 1–8.
- [43] G. F. Riley and T. R. Henderson, *The ns-3 Network Simulator*. Berlin, Heidelberg: Springer Berlin Heidelberg, 2010, pp. 15–34.

- [44] A. Larsson, A. Piotrowski, T. Giles, and D. Smart, "Near-earth RF propagation - Path loss and variation with weather," in *2013 International Conference on Radar*, Sept 2013, pp. 57–63.
- [45] D. Halperin, B. Greenstein, A. Sheth, and D. Wetherall, "Demystifying 802.11n power consumption," in *Proceedings of the 2010 International Conference on Power Aware Computing and Systems*, ser. HotPower'10. Berkeley, CA, USA: USENIX Association, 2010.



**Varun Amar Reddy** received the B.Tech. degree in Electronics and Communication Engineering from the National Institute of Technology Karnataka, Surathkal, India in 2016. He is currently pursuing the Ph.D. degree in Electrical and Computer Engineering with the Georgia Institute of Technology, Atlanta, USA. His research interests lie broadly in wireless communications and networking, with a focus on wireless LAN, channel access protocols, and energy-efficient resource allocation.



**Gordon L. Stüber** (S'81-M'82-SM'96-F'99) received the B.A.Sc. and Ph.D. degrees in electrical engineering from the University of Waterloo, Waterloo, ON, Canada, in 1982 and 1986, respectively. In 1986, he joined the School of Electrical and Computer Engineering, Georgia Institute of Technology, where he is the Joseph M. Pettit Chair Professor in Communications.

He is the author of the wireless textbook *Principles of Mobile Communication* (Kluwer Academic Publishers, 1996, 2/e 2001, 3/e 2011, 4/e 2017). He was a co-recipient of the Jack Neubauer Memorial Award in 1997 for the best systems paper published in the IEEE Transactions on Vehicular Technology and the Neal Shepherd Memorial Best Propagation Paper Award in 2012, for the best propagation paper published in the IEEE Transactions on Vehicular Technology. He became an IEEE Fellow in 1999 "for contributions to mobile radio and spread spectrum communications." He was the recipient of the IEEE Vehicular Technology Society James R. Evans Avant Garde Award in 2003 "for his contributions to theoretical research in wireless communications," the 2007 IEEE Communications Society Wireless Communications Technical Committee Recognition Award "for outstanding technical contributions in the field and for service to the scientific and engineering communities," and the 2017 IEEE ComSoc RCC Technical Recognition Award "for outstanding research contributions to radio communications," and the IEEE Vehicular Technology Society Outstanding Service Award in 2005. He was an IEEE Communication Society Distinguished Lecturer (2007–2008) and IEEE Vehicular Technology Society Distinguished Lecturer (2010–2012).

Dr. Stüber was the Technical Program Chair for the 1996 IEEE Vehicular Technology Conference (VTC'96), the Technical Program Chair for the 1998 IEEE International Conference on Communications (ICC'98), the General Chair of the Fifth IEEE Workshop on Multimedia, Multiaccess and Teletraffic for Wireless Communications (MMT'00), the General Chair of the 2002 IEEE Communication Theory Workshop (CTW'02), and the General Chair of the Fifth YRP International Symposium on Wireless Personal Multimedia Communications (WPMC'02). He is a past Editor for Spread Spectrum with the IEEE Transactions on Communications (1993–1998), a past member of the IEEE Communications Society Awards Committee (1999–2002). He was an elected Member-at-Large on the IEEE Communications Society Board of Governors (2007–2009), and is an elected member of the IEEE Vehicular Technology Society Board of Governors (2001–2018).



**Suhail Al-Dharrab** received his B.Sc. degree in Electrical Engineering from King Fahd University of Petroleum and Minerals, Dhahran, Saudi Arabia in 2005. He received the M.A.Sc. and Ph.D. degrees in Electrical and Computer Engineering from University of Waterloo, Waterloo, Canada, in 2009 and 2013, respectively. From 2005 to 2007, he was a Graduate Assistant in the Electrical Engineering Department at King Fahd University of Petroleum and Minerals. In 2015, he was a Visiting Professor in the School of Electrical and Computer Engineering at the Georgia Institute of Technology, Atlanta, USA. He is currently an Assistant Professor in the Electrical Engineering Department and Assistant Dean of Research at King Fahd University of Petroleum and Minerals, Dhahran, Saudi Arabia. His research interests span topics in the areas of wireless communication systems, underwater acoustic communication, digital signal processing, and information theory.



**Wessam Mesbah** (M'09-SM'15) received the M.Sc. and B.Sc. degrees (Hons.) in electrical engineering from Alexandria University, Alexandria, Egypt, in 2003 and 2000, respectively, and the Ph.D. degree from McMaster University, Hamilton, ON, Canada, in 2008. From 2009 to 2010, he was a Post-Doctoral Fellow with Texas A&M University, Doha, Qatar. He joined the Electrical Engineering Department, King Fahd University of Petroleum and Minerals, in 2010, where he is currently an Associate Professor. His research interests include cooperative communications and relay channels, layered multimedia transmission, wireless sensor networks, multiuser MIMO/OFDM systems, cognitive radio, optimization, game theory, and smart grids.



**Ali H. Muqaibel** (M'03-SM'12) received the B.Sc. and M.Sc. degrees from the King Fahd University of Petroleum and Minerals (KFUPM), Dhahran, Saudi Arabia, in 1996 and 1999, respectively, and the Ph.D. degree from the Virginia Polytechnic Institute and State University, Blacksburg, Virginia, in 2003. During his study at Virginia Tech, he was with both the Time Domain and RF Measurements Laboratory and the Mobile and Portable Radio Research Group. He is currently an Associate Professor with the Electrical Engineering Department, KFUPM. He was a Visiting Associate Professor with the Center of Advanced Communications, Villanova University, Villanova, PA, USA, in 2013, a Visiting Professor with the Georgia Institute of Technology in 2015, and a Visiting Scholar with King Abdullah University for Science and Technology (KAUST), Thuwal, Saudi Arabia in 2018. He has authored two book chapters and over 100 articles. His research interests include the direction of arrival estimation, through-wall-imaging, localization, channel characterization, and ultra-wideband signal processing. He received many awards in the Excellence in teaching, advising, and instructional technology.